A multi-scale model for the modulation and rectification of the ITCZ

Joseph A. Biello *

Department of Mathematics, University of California, Davis, CA

Andrew J. Majda

Courant Institute of Mathematical Sciences, Center for Atmosphere-Ocean Science,

New York University , New York, NY

* *Corresponding author address:* Joseph A. Biello, Department of Mathematics, University of California, 1 Shields Ave., Davis, CA 95616, email: biello@math.ucdavis.edu

ABSTRACT

We introduce the modulation of the ITCZ equations (M-ITCZ) which describe the multi-scale dynamics of the ITCZ on one day to one month time scales in which mesoscale convectively coupled Rossby waves in the ITCZ are modulated by a large scale gravity wave which is also generated by convection. Westward propagating disturbances are observed to cause ITCZ breakup over the course of a few days, and the M-ITCZ meso/planetary scale coupled waves provide a mechanism for this interaction, thereby providing a framework to study the modulation and rectification of the Hadley circulation over long zonal length scales in the ITCZ.

We consider examples of zonally symmetric heating profiles in the M-ITCZ system and generate a Hadley circulation consistent with the observed winds. Zonally localized heating creates a wind response throughout the tropics which is carried by a pair of zonally propagating gravity bores driving mean easterlies at the base and mean westerlies at the top of the troposphere. The bores carry low temperature/upward velocity perturbations to the west of the heating and high temperature and downward velocity perturbations to the east making the westward propagating branch favorable to convective triggering and the eastward propagating branch favorable to convective suppression.

The mesoscale dynamics of the M-ITCZ describe convectively forced, nonlinear Rossby waves propagating in the zonal winds created by the planetary scale gravity wave. We suggest that convective coupling slows the westward propagating gravity wave, thereby creating a coupled gravity/Rossby wave which is

similar to the westward propagating disturbances seen in the ITCZ.

1. Introduction

The meridional overturning circulation driven by diabatic heating in the tropics is a fundamental aspect of tropical dynamics. When considered in its zonal mean, it is called the Hadley circulation (Held and Hou 1980). However, zonal variations of the circulation, the Walker Circulation, are as significant as the zonal variations in tropical precipitation which drive them. The ascending branch of this circulation is called the intertropical convergence zone (ITCZ), and is meridionally confined near the equator where deep convection is most prominent. The ITCZ, itself, is not a stationary structure by any means. In the west Pacific it migrates meridionally with the seasonal cycle while in the east Pacific it tends to remain at northern latitudes. On yet shorter timescales, the ITCZ demonstrates even more dramatic variability with embedded westward propagating disturbances (Chang 1970) and its periodic breaking up into nascent tropical cyclones and then reforming over the course of several weeks (Hack et al. 1989).

There are two main mechanisms which have been used to explain the Pacific ITCZ breakup; vortex rollup (Hack et al. 1989; Ferreira and Schubert 1997) and the westward propagating disturbances themselves (Gu and Zhang 2001, 2002; Wang and Magnusdottir 2006). The vortex rollup mechanism amounts to barotropic/baroclinic instabliity of a diabatically forced zonal wind profile. In a recent observational study of the central and eastern Pacific by Wang and Magnusdottir (2006), the vortex rollup mechanism was identified as the primary cause of ITCZ breakdown in the central Pacific. In that study, vortex rollup tends to create several weak tropical vortices from the ITCZ which often dissipate quickly thereby allowing a reformation of the ITCZ within a few days.

In that same study (Wang and Magnusdottir 2006) it was found that westward propagating disturbances also had the effect of disrupting the ITCZ, but with a resultant formation of one or two tropical depression strength vorticies. Furthermore, these disturbances tend to be concentrated in the eastern Pacific near the Mexican coast. Spectral analysis of the ITCZ shows that the wave signal is dominated at long zonal wavelengths by these westward propagating disturbances (Gu and Zhang 2001). However, the coupling between modulations in ITCZ strength and the strength of disturbances depends on the zonal location of the disturbances (Gu and Zhang 2002; Wang and Magnusdottir 2006) and whether the ITCZ owes its existence to the waves (Chang 1973), or simply generates the waves is not fully understood. These observational and model studies, as well as idealized numerical experiments (Horinouchi 2012) lend evidence to the notion that it is essential to understand fast, transient wave dynamics in order to understand the ITCZ and the Hadley circulation in general.

The aim of this paper is to present a model which captures the dynamics of the ITCZ on meso- and planetary scales and on timescales which are able to resolve the embedded waves (one to several days). Using the techniques of multiple scales asymptotics, we will systematically derive the modulation equations for the ITCZ (hereafter referred to as the M-ITCZ equations). Then we will discuss the properties of these equations and, in particular, the properties of the large scale gravity waves that they describe. The large scale gravity wave is shown to be generated through meso-scale convective activity and, by modulating the mean zonal winds, thereby also modulates the mesoscale convection.

The work of Sobel et al. (2001) codified the assumption of earlier authors that the tropical atmosphere is in a state with weak zonal temperature gradients; this has been named

the weak temperature gradient approximation and will be hereafter referred to as WTG. Its primary consequence is that, on large scales in the tropics, the vertical transport of the potential temperature stratification is approximately equal to the diabatic heating, thereby removing the thermal inertia terms and changing the temperature equation from a prognostic, to a diagnostic for the horizontal convergence (Polvani and Sobel 2002; Burns et al. 2006).

Majda and Klein (2003) used multiscale asymptotics to show show that, as a consequence of the strength of diabatic heat sources relative to the equatorial Coriolis terms, the WTG approximation is valid on equatorial mesoscales (several times 500 km in the horizontal directions) as long as mean diabatic heating rates on these scales do not exceed 33 Kelvin/day; the theory they derived is called the mesoscale equatorial weak temperature gradient, MEWTG. Since MEWTG is valid on scales much smaller than the circumference of the Earth, MK showed that the dynamics could be modulated over planetary scales by the addition of a zonally modulated pressure. Such a weak gradient of pressure also necessitates a weak temperature gradient in the zonal directions, however the original MEWTG theory did not provide a means for determining this weaker temperature gradient.

In the second section, we provide a systematically derived closure for the weak temperature gradient on the equatorial mesoscales, called the modulational ITCZ equations (M-ITCZ). In the third section, we will study the planetary scale interaction of the meridional overturning circulation and this new gravity wave. The planetary scale means and mesoscale fluctuations can be easily separated in the M-ITCZ theory to describe the interaction of mesoscale eddies with the large scales. Though the theory is completely non-linear (no separation between mesoscale fluctuations and planetary means), the large scales can be

studied in the presence of prescribed diabatic heating and upscale momentum fluxes.

The existence of the gravity wave along the ITCZ has important implications for the modulation and rectification of the ITCZ itself. Generated as a response to convection, the wave carries opposite temperature and vertical velocity perturbations to the west than it does to the east. The westward traveling portion of the wave carries conditions favorable to convective triggering (cold temperatures and uplifting (Mapes 1993; Houze 1997; Stechmann and Majda 2009)) whereas the eastward branch carries conditions favorable to convective suppression. This has possible ramifications for zonal correlations of convection at large separations in the tropics.

In the final section we give a simple physical explanation for the gravity wave, compare the M-ITCZ theory to the classical Matsuno-Gill models and discuss future directions of this research.

2. The ITCZ modulated by convectively initiated gravity waves

a. Summary of the M-ITCZ theory

We leave the derivation of the M-ITCZ equations to section 2d, but present them here in order to discuss properties of the equations in the following subsections

$$\begin{aligned}
\frac{D}{Dt}u - y\,v =& -p_x - \Pi_X + S_u \\
\frac{D}{Dt}v + y\,u =& -p_y + S_v \\
w =& S_\theta \\
u_x + v_y + w_z =& 0 \\
\Pi_x = \Pi_y = 0, \quad \Pi_z =& \Theta \\
\Theta_t + \langle\overline{w}\rangle\,\Theta_z + W =& 0 \\
[\langle\overline{u}\rangle - U]_X + W_z =& 0.
\end{aligned} \tag{1}$$

where the advective derivative is taken with respect to the total circulation, (u, v, w).

The M-ITCZ equations (1) along with the definitions of the averages in (15), (16) and (20) constitute a closed system of seven equations for the seven variables $(u, v, w, W, \Pi, p, \Theta)$. At lowest order they describe flows in the tropical belt (around the ITCZ) which are in weak temperature gradient balance with imposed heating. They are valid on the equatorial mesoscales; (x, y) are measured in units of 500 km. The unit of horizontal and vertical velocity are 5 m/s and 5 cm/s, respectively. Bars denote zonal mesoscale averages, angle

brackets denote meridional mesoscale averages and U is the vertical average of $\langle \overline{u} \rangle$. The M-ITCZ equations are valid if the flows, filtered on the mesoscales, remain order one in these units; this is to say that the flows remain within a few multiples of the unit of horizontal or vertical velocity.

Figure 1 shows a schematic of the equatorial belt up to a poleward distance L_* where the equations are valid. The nonlinear theory described by the first four equations in (1) can drive mean zonal flows, u, within a mesoscale box, and since there are many widely separated such boxes across the equatorial belt, this mean flow can vary over zonal distances much larger then the mesoscales. The large scale zonal variable X is introduced to describe the scale of this modulation.

The secondary flow, W is not in WTG balance. M-ITCZ allows for a strong pressure perturbation, Π, in hydrostatic balance with the temperature perturbation, Θ, which is measured in units of 3.3 Kelvin. The constraints on the fifth line of (1) require that the temperature perturbation vary neither on the zonal mesoscales, nor in the meridional direction in the deep tropics, though it can evolve in time. Together, the first and sixth lines in (1) describe a gravity wave propagating zonally in the tropics. The final equation requires that the secondary circulation, W, be in zonal/vertical incompressible balance with the baroclinic component of the mesoscale averaged zonal wind.

b. Separation into large scale means and fluctuations in the equatorial belt

Notice that the gravity wave arises because of the coupling of temperature and pressure, Θ, Π, with the derivative of the mean zonal velocity, $\langle \overline{u} \rangle_X$, and the secondary vertical velocity,

142 W_z. By its nature the wave carries perturbations which vary on neither the zonal nor
143 meridional mesoscales, which is to say that it is a large scale modulational wave that is
144 independent of latitude in the deep tropics.

145 It is instructive, therefore, to separate all of the functions (with the exception of Θ and Π
146 which have no mesoscale fluctuations) into mesoscale zonal mean components plus mesoscale
147 fluctuations,

$$u \equiv \overline{u} + u', \quad \text{etc..} \tag{2}$$

148 We only consider a separation into zonal means and fluctuations, not meridional means. This
149 is a result of the fact that, in the zonal direction, we have created a truly multiscale theory
150 - fluctuations on the x-scale and modulations on the X-scale. Whereas in the meridional
151 direction, the equatorial layer has a finite extent, L_*, as we will discuss in the derivation
152 (see the schematic in figure 1). The resulting equations for the modulation of the mesoscale
153 zonal mean flow on the planetary scale are

$$\begin{aligned}
\overline{u}_t + (\overline{v}\,\overline{u})_y + (\overline{w}\,\overline{u})_z - y\,\overline{v} &= -\Pi_X + \overline{S_u} - \left(\overline{v'\,u'}\right)_y - \left(\overline{w'\,u'}\right)_z \\
\overline{v}_t + (\overline{v}\,\overline{v})_y + (\overline{w}\,\overline{v})_z + y\,\overline{u} &= -\overline{p}_y + \overline{S_v} - \left(\overline{v'\,v'}\right)_y - \left(\overline{w'\,v'}\right)_z \\
\overline{w} &= \overline{S_\theta} \\
\overline{v}_y + \overline{w}_z &= 0.
\end{aligned} \tag{3}$$

154 Notice that the mean fields are coupled to the mesoscale fluctuations by meridional and
155 vertical components of the Reynolds stress. The equations for the large scale temperature
156 perturbation and the secondary vertical flow remain unchanged from (1).

157 Subtracting the mean circulation equations (3) from equations (1) yields the equations

for the mesoscale fluctuations

$$\begin{aligned}
\frac{\overline{D}}{\overline{D}t}u' + v'\,\overline{u}_y + w'\,\overline{u}_z - y\,v' &= -p'_x + S'_u - \left[u'\,u'_x + v'\,u'_y + w'\,u'_z - \left(\overline{v'\,u'}\right)_y - \left(\overline{w'\,u'}\right)_z\right] \\
\frac{\overline{D}}{\overline{D}t}v' + v'\,\overline{v}_y + w'\,\overline{v}_z + y\,u' &= -p'_y + S'_v - \left[u'\,v'_x + v'\,v'_y + w'\,v'_z - \left(\overline{v'\,v'}\right)_y - \left(\overline{w'\,v'}\right)_z\right] \\
w' &= S'_\theta \\
u'_x + v'_y + w'_z &= 0
\end{aligned} \tag{4}$$

where the advective derivative is taken with respect to the mean flow

$$\frac{\overline{D}}{\overline{D}t} = \partial_t + \overline{u}\,\partial_x + \overline{v}\,\partial_y + \overline{w}\,\partial_z. \tag{5}$$

The third equation in (4) states that the mesoscale fluctuations are also in WTG balance with the fluctuating heating, S'_θ. The mean flow acts to advecte and stretch the mesoscale velocity fluctuatinons as seen in the first two lines of (4).

c. Properties of the M-ITCZ equations

The system of equations as written in (3), the last three lines in (1) and (4) is no easier to solve than the whole M-ITCZ system of equations in (1), however the separation into means and fluctuations does illuminate some features of the theory.

The first feature is that the theory is completely non-linear - there is no separation of strengths, nor separation of time scales between mean flows and fluctuations which would facilitate a simple linear solution to the fluctuation equations (4). The second is that both large and small scale flows are driven by direct heating on their respective scales; there are

no upscale temperature fluxes in this theory in contrast to the IPESD theory in MK and IMMD in Biello and Majda (2010).

The third is that the relevant momentum forcing is measured in units of 5 m/s/day. Were we to consider a momentum drag law of the form $S^u = -C\,u$, $S^v = -Cv$ and using estimates of cumulus friction which suggest 3-5 day timescales at their strongest (Lin et al. 2005), then $C \approx 0.2 - 0.3$. So momentum damping corresponds to an order 1 term in this theory and can be included when studying solutions to the M-ITCZ equations.

The fourth point is that the second equation in (3) determines the zonal mean of the first order pressure, $\overline{p}$, from the velocity field and forcing; therefore it is a diagnostic equation for $\overline{p}$, not a prognostic equation for $\overline{v}$. In the following section we focus attention on the zonal mesoscale fields in the presence of specified heating, momentum forcing and upscale fluxes, so the second equation in (3) does not need to be solved.

Fifth, we note that the system of equations for the zonal mesoscale mean flow (3) requires boundary conditions at the meridional limit of the deep tropics. The third equation describes a mean vertical velocity which is in WTG balance with the heating. To solve for the meridional velocity, simply integrate in the meridional direction

$$\overline{v}(y,z,X,t) = \overline{v}(L_*,z,X,t) + \int_y^{L_*} \left(\overline{S_\theta}\right)_z (y',z,X,t)\, dy \tag{6}$$

and realize that $\overline{v}(L_*,z,X,t)$ is not determined by the theory. Ultimately, the meridional component of the flow in the M-ITCZ theory must be matched to a meridional flow coming from higher latitiudes; we leave this matching for a subsequent paper. In the examples of the following section we are interested in studying the waves which emerge in the deep tropics

so we will assume a closed meridional circulation so that $\overline{v} = 0$ at the meridional boundaries of the tropics.

Sixth, consider the linear theory of the planetary flows. In the absence of thermal forcing $\overline{w} = 0$ and, using no flux boundary conditions at L_* then $\overline{v} = 0$, also. Therefore equations (3) and the last three lines of (1) describe a linear gravity wave (possibly forced by upscale fluxes of zonal momentum) whose circulation is independent of latitude, traveling both east and westward along the ITCZ.

Conversely, the linearization of (4) in the absence of forcing and mean flow $(\overline{u}, \overline{v}, \overline{w})$ is

$$\begin{aligned} u'_t - yv' + p'_x &= 0 \\ v'_t + yu' + p'_y &= 0 \\ u'_x + v'_y &= 0. \end{aligned} \tag{7}$$

As noted in MK, though these equations have no vertical derivatives, they describe flows which depend on z and these mesoscale flows have the dispersion relation of barotropic Rossby waves on a β-plane. As such, the M-ITCZ theory can describe the coupling between equatorial mesoscale circulation and extratropical Rossby waves.

Lastly, the interaction of the planetary scale gravity wave with the mesoscale Rossby dynamics suggest the following mechanism for modulation and rectification of the ITCZ. Convection in the ITCZ generates mesoscale dynamics (such as Rossby waves) which drives a large scale gravity wave. The gravity wave carries temperature and vertical velocity perturbations which can excite convection elsewhere in the tropics, thereby modulating the ITCZ at distances much greater than the mesoscales.

209 In a convectively coupled model the heating, S_θ, depends on the temperature and mois-
210 ture fields and is the method by which forced mesoscale Rossby waves drive the planetary
211 scale gravity wave. Since the Rossby waves propagate westward, it is plausible that they
212 are strongly tied to the westward propagating gravity wave. Furthermore, as we shall show
213 in section 3, the westward propagating wave carries perturbations which are favorable to
214 convective triggering, thereby providing the source for the mesoscale Rossby waves.

215 *d. Derivation of M-ITCZ*

216 The mesoscale equatorial weak temperature gradient equations (MEWTG) were derived
217 by Majda and Klein (2003) to describe the modulations to the weak temperature gradient
218 approximation (Bretherton and Sobel 2003) which can arise from the effects of nonlinear
219 advection. They are valid on the equatorial mesoscales (500 km in the horizontal directions)
220 so long as diabatic heat sources do not significantly exceed 33 Kelvin/day when averaged
221 on these scales. The derivation outlined below begins with the hydrostatic, incompressible
222 equatorial primitive equations; this starting point allows us to arrive at the simplified system
223 in fewer steps than MK without neglecting any of the salient effects (Majda et al. 2008),
224 much like the derivation of the IPESD equations in Majda (2007); Biello and Majda (2006,
225 2010).

226 We begin with the incompressible, hydrostatic primitive equations on the equatorial β-
227 plane. Consider an atmosphere with a buoyancy frequency of $N = 10^{-2}\,\mathrm{s}^{-1}$, troposphere
228 height $H_T = \pi H$ where $H = 5\,\mathrm{km}$ so that the dry gravity wave speed is $c = NH =$
229 $50\,\mathrm{m/s}$. the adiabatic lapse rate is $\Gamma = 6.5\,\mathrm{K/km}$ and the Coriolis parameter is $\beta = 2.27 \times$

$10^{-11}\,(\mathrm{ms})^{-1}$. We non-dimensionalize the horizontal length scales using L and the time scale using T, so that horizontal velocities are measured in units of L/T . In order that the Coriolis force and pressure gradient participate in the equations at lowest order, it is required that $\beta\, L\, T = 1$, and that the pressure be measured in units of L^2/T^2. If we fix L to be on the mesoscales, $L = 500\,\mathrm{km}$, then $T \approx 1\,\mathrm{day}$. Equivalently, we could have sought variations on the diurnal time scale, $T = 1\,\mathrm{day}$, and realized that the appropriate length scale over which the Coriolis force is in balance with advection and pressure forces is $L = 500\,\mathrm{km}$. Therefore the horizontal velocities are measured in units of $L/T = 5\,\mathrm{m/s}$ and the vertical velocity is measured in units of $H/T = 5\,\mathrm{cm/s}$.

The ratio of typical horizontal velocities to the dry gravity wave speed is a small parameter which will define as

$$\epsilon \equiv \frac{L/T}{c} = \frac{L/T}{NH} = \frac{5\,\mathrm{m/s}}{50\,\mathrm{m/s}} = 0.1 \ll 1. \tag{8}$$

Using the equation of hydrostatic balance, the buoyancy frequency and the lapse rate, we find that the temperature perturbations are measured in units of $\theta_0 = \Gamma\, H\, \epsilon^2 \approx 0.33\,\mathrm{K}$. Therefore, the non-dimensionalized primitive equations become

$$\begin{aligned} \frac{D}{Dt}u - y\,v &= -p_x + S_u \\ \frac{D}{Dt}v + y\,u &= -p_y + S_v \\ \epsilon^2\frac{D}{Dt}\theta + w &= S_\theta \\ p_z = \theta, \qquad & u_x + v_y + w_z = 0 \end{aligned} \tag{9}$$

where the advective derivative is $\frac{D}{Dt} = \frac{\partial}{\partial t} + u\frac{\partial}{\partial x} + v\frac{\partial}{\partial y} + w\frac{\partial}{\partial z}$. In this non-dimensionalization, momentum sources are measured in units of $5\,\mathrm{m/s/day}$ and the diabatic heat source is

measured in units of 33 K/day. This framework allows the heating rate to be not larger than about 33 K/day, but it can be smaller. However a much smaller heating rate (say, order ϵ) can only be balanced by a much smaller vertical velocity (again, order ϵ) which would render the flow incompressible in the horizontal direction at lowest order. While this is not an uninteresting scenario, it arises as a specific case of the more general theory.

The weak temperature gradient approximation is simply the primitive equations (9) with $\epsilon = 0$, so that the advection of potential temperature is neglected. In this limit the vertical advection of the background temperature stratification is balanced by the diabatic heating rate and the temperature is determined from the pressure using the hydrostatic approximation.

1) Multiple scales and asymptotic solution strategy

There are several mesoscale regions across the equatorial circumference (see figure 1) and the equations in (9) govern the dynamics in each such region. A priori, we can expect that a mean circulation and temperature can arise in some longitude band that is significantly different than the flow and temperature on the other side of the globe. That is to say, the mesoscale dynamics can be modulated over planetary scales. In the framework of multiple scales asymptotics, this larger scale is introduced as a second independent variable related to the original zonal variable through

$$X = \epsilon x \tag{10}$$

and thereby measures zonal lengths in the tropics in units of $L_P = 5000\,\mathrm{km}$. All of the dynamical variables then become functions of X also, specifically $u(x, \epsilon x, y, z, t) =$

266 $u(x, X, y, z, t)$, etc. for the other variables and zonal derivatives are replaced by their multi-
267 scale counterparts

$$\frac{\partial}{\partial x} \longrightarrow \frac{\partial}{\partial x} + \epsilon \frac{\partial}{\partial X}. \tag{11}$$

268 Refer to figure 1 for a schematic of the multi-scale domain.

269 Since it is the zonal pressure gradient, not the pressure itself, which participates in the
270 dynamics, it is necessary to allow for a stronger pressure perturbation which can have a
271 gradient on the zonal planetary scales, but not on the zonal mesoscales. The fact that it
272 cannot have gradients on the mesoscale will arise naturally from the asymptotic solution as
273 we will show below.

274 Now we seek an asymptotic solution $(u^\epsilon, v^\epsilon, w^\epsilon, p^\epsilon, \theta^\epsilon)$ of the primitive equations in (9)
275 where the x-derivatives are replaced by their multi-scale counterparts in (11) and the vari-
276 ables have the following asymptotic expansion

$$\begin{aligned} &u^\epsilon = u + \epsilon\, u_1, \qquad v^\epsilon = v + \epsilon\, v_1 \qquad w^\epsilon = w + \epsilon\, w_1 \\ &\theta^\epsilon = \epsilon^{-1}\,\Theta + \theta + .., \quad p^\epsilon = \epsilon^{-1}\,\Pi + p + ... \end{aligned} \tag{12}$$

277 The stronger temperature pertubation, Θ is measured in units of $3.3\,\mathrm{K}$ and the stronger
278 pressure perturbation is measured in units of $250\,(\mathrm{m/s})^2$.

279 2) $O(\epsilon^{-1})$

280 The lowest order terms in equations (9) are singular in ϵ and dictate that the lowest order
281 pressure only depends on height and the planetary scale coordinate

$$\Pi_x = \Pi_y = 0. \tag{13}$$

282 and the pressure is in hydrostatic balance with the temperature

$$\Pi_z = \Theta, \tag{14}$$

283 meaning Θ also does not vary on the horizontal mesoscales. This is exactly the statement
284 of the weak temperature gradient approximation discussed by Bretherton and Sobel (2003),
285 that the tropics cannot sustain temperature gradients as large as 3.3 K on the tropical
286 mesoscales. Had we introduced a stronger temperature perturbation in (12), this result
287 would still hold for that stronger temperature. However, we will see below that the temper-
288 ature scale described by Θ will interact dynamically with the MEWTG theory, a stronger
289 temperature variation would not.

290 Since the lowest order temperature and pressure perturbations are independent of both
291 the zonal and meridional mesoscales coordinates, they describe the modulation to the mean
292 temperature and pressure perturbation in each mesoscale box. In order to close the resulting
293 equations for Θ and Π we will need to define two averages, the zonal mesoscale average

$$\overline{f}(y,z,X,t) \equiv \lim_{L\to\infty} \frac{1}{2L} \int_{-L}^{L} f(x,y,z,X,t)\, dx \tag{15}$$

and the meridional mesoscale average

$$\langle f \rangle (x, z, X, t) \equiv \frac{1}{2L_*} \int_{-L_*}^{L_*} f(x, y, z, X, t)\, dy \tag{16}$$

where L_* measures the poleward extent of the equatorial β-plane. Notice that the zonal average is taken over an infinite zonal mesoscale domain, which is a consequence of the multi-scale ansatz of separation of scales in the zonal direction. For the purpose of comparison with observations, this average can be effectively thought of as a windowed average, or filtering over the zonal mesoscales.

On the other hand, the meridional average is to be taken over a finite domain in the meridional direction, $2L_*$, which is the meridional extent of the region of strong convection, the ITCZ. At this stage in the derivation L_* is left arbitrary, but with some restrictions. Ultimately, L_* must be $O(1)$, which is to say that we cannot extend this theory to latitudes where y (which is measured in units of 500 km) is large. An a posteriori check on the results would set the value of L_* at the boundary of the latitudinal band where the non-dimensionalized zonal and meridional flows and temperature perturbations all remain $O(1)$ - in particular the theory is no longer valid at latitudes where the meridional gradient of temperature is large, thereby failing to be WTG.

3) $O(\epsilon^0)$: MEWTG

Collecting terms of order ϵ^0 in the velocity, temperature and incompressibility equations, we arrive at the first four lines of equation (1) in the M-ITCZ theory. These are the MEWTG

equations which were first derived in MK and subsequently discussed in Dolaptchiev (2005); Majda et al. (2008). However at this point Π and Θ are arbitrary except for the constraints that they not vary on the mesoscales (13) and hydrostatic balance (14).

4) $O(\epsilon^1)$: Closing the equation for Θ and Π

We need an equation for Θ in order to close the MEWTG equations. Consider the temperature equation in (9) evaluated at first order in ϵ. Taking its zonal and meridional mesoscale average we find

$$\Theta_t + \langle \overline{w} \rangle \Theta_z + \langle \overline{w_1} \rangle = \left\langle \overline{S_{1,\theta}} \right\rangle \tag{17}$$

where we have used the fact that Θ is independent of (x, y). An equation for the secondary vertical flow is obtained by taking the zonal and meridional average of the incompressibility constraint at first order,

$$\langle \overline{u} \rangle_X + \langle \overline{w_1} \rangle_z = -\frac{\overline{v_1}(L_*, z, X, t) - \overline{v_1}(-L_*, z, X, t).}{2L_*} \tag{18}$$

Equations (17) and (18) still do not close the system since there is no equation for the difference in $\overline{v_1}$ at the poleward boundaries of the tropical layer. In order to close the M-ITCZ system, we must specify a method to solve for this secondary flow. The right hand side of (18) describes a net inflow into the equatorial layer, but it is a secondary inflow; the MEWTG theory does not require that v (the primary inflow) be zero at $y = \pm L_*$. It is natural to absorb any flux from outside the equatorial layer into the primary flow, thereby providing matching conditions for v, but not for $\overline{v_1}$. On the other hand, just setting $\overline{v_1} = 0$

329 at the meridional boundaries is not possible since a zonal variation in the vertical mean of
330 the meridional mean zonal velocity, $\langle \overline{u} \rangle_X$, would then drive a net vertical outflow from the
331 top or bottom boundary of the layer.

332 Denote the right hand side of (18) as $\eta(z, X, t)$; $\eta > 0$ ($\eta < 0$) corresponds to a secondary
333 inflow (outflow). A closed theory will provide an algorithm to calculate η. The principle we
334 use is that η responds only to the dynamics internal to the deep tropical layer. It will be
335 used to absorb the mean of the higher order heating and, more importantly, it will be used
336 to ensure that the constraint on the left hand side of (18) describes incompressibility in the
337 zonal/vertical directions alone. We emphasize that this assumption is not restrictive since
338 any inflow into the ITCZ can be incorporated into the lower order meridional velocity, v.

339 Define a residual vertical circulation

$$W(z, X, t) \equiv \langle \overline{w_1} \rangle - \left\langle \overline{S_{\theta,1}} \right\rangle \tag{19}$$

340 and the barotropic component of the mesoscale mean zonal velocity

$$U(X, t) \equiv \frac{1}{\pi} \int_0^\pi \langle \overline{u} \rangle (z, X, t)\, dz. \tag{20}$$

341 Upon substituting these definitions into (18) we can write

$$[\langle \overline{u} \rangle - U]_X + W_z = \eta - U_X - \left\langle \overline{S_{\theta,1}} \right\rangle_z . \tag{21}$$

342 To calculate the mean secondary inflow, η we require the right hand side of (21) be equiva-

lently zero

$$\eta = U_X + \left\langle \overline{S_{\theta,1}} \right\rangle_z \tag{22}$$

meaning that zonal variations in the barotropic zonal velocity and mean higher order heating (right hand side) drive a secondary outflow from the equatorial layer (left hand side). Using equation (22) in (21) it is straightforward to see that, given $\langle \overline{u} \rangle$, the vertical velocity can be calculated so that the secondary flow does not penetrate the upper or lower boundaries of the troposphere. Finally the temperature and incompressibility constraints become those of the last two lines of equation (1). This completes the derivation of the M-ITCZ equations.

3. Zonally modulated heating and large scale gravity waves

In this section we consider the planetary scale equations in isolation from the upscale fluxes of momentum, as well as any meridional fluxes from outside the ITCZ. Since we are most interested in how convection in the ITCZ can modulate convection elsewhere in the ITCZ, we focus on thermal forcing in this paper, leaving zonal momentum forcing for future work. In order to have a closed poleward circulation, we require $\overline{v}(L_*, z, X, t) = \overline{v}(-L_*, z, X, t) = 0$ which, because of vertical/meridional incompressibility implies that the meridional average of the vertical velocity is zero, $\langle \overline{w} \rangle = 0$. Due to the WTG nature of the circulation, this further requires that the heating has zero meridional average at every height and longitude, $\left\langle \overline{S_\theta} \right\rangle (z, X, t) = 0$.

Additionally, we include momentum damping consistent with stronger damping in the

lower troposphere, $d(z)$, in order to model boundary layer drag as is needed in realistic models of the Hadley circulation (Held and Hou 1980). In all of the examples in the subsequent sections, the drag coefficient is

$$d(z) = d_0\, e^{-z/H_d} \tag{23}$$

with $d_0 = H_d = 1$. This corresponds to a 1 day drag timescale at the base of the troposphere exponentially increasing to 23 days at the top of the troposphere. In this scenario, the equations on the planetary scale simplify to

$$\begin{aligned} \overline{u}_t + (\overline{v}\,\overline{u})_y + (\overline{w}\,\overline{u})_z - y\,\overline{v} + \Pi_X &= -d\,\overline{u} \\ \overline{w} &= \overline{S_\theta} \\ \overline{v}_y + \overline{w}_z &= 0 \\ \Theta_t + W &= 0, \quad \Pi_z = \Theta \\ [\langle \overline{u} \rangle - U]_X + W_z &= 0 \end{aligned} \tag{24}$$

plus the constraints that Π and Θ be independent of latitude (the fifth line in equation 1).

Before turning to example solutions, let us consider steady thermal and momentum forcing of equations (24). The steady nature of the temperature equation requires that the meridional mean secondary vertical velocity, W, be zero for all heights and longitudes which further implies that the vertical shear of the meridional mean zonal wind is independent of X,

$$[\langle \overline{u} \rangle_z]_X = 0. \tag{25}$$

After the onset of convection at a particular longitude a gravity bore propagates zonally

away from the convective region. It modifies the zonal wind so that, in equilibrium, there is no zonal variation in the meridional mean of the vertical shear of zonal wind. This is a crucial property of the equations and it suggests the *raison d'etre* of the gravity wave, to equilibrate the mean vertical shear everywhere in the ITCZ. We will see how this manifests itself in the examples which follow.

We consider three examples differentiated by the zonal, meridional and vertical structure of their heating. The first group considers zonally symmetric heating in three cases; equinox heating/cooling, equinox heating with antisymmetric cooling, boreal winter heating/cooling; the meridional profile of the heating and their resulting stream functions are shown in figure 2. The vertical structure of the heating is simply the first baroclinic mode ($\propto \sin(z)$) and these examples are meant to consider the effects of deep tropospheric convection on the circulation. There can be no gravity wave in this case, so the example is included to show the behavior of the equilibrium zonal winds. The second example uses zonally localized heating in an equinox setting and because of the sharp localization of the heating, the gravity wave will appear most prominent. The third example also has zonally localized, equatorially symmetric heating, however the circulation is concentrated in the lower troposphere and is meant to mimic a congestus heating profile ($\propto \sin(z) + \sin(2z)/2$) (Biello and Majda 2005). In all examples, the heating is turned on impulsively at $t = 0$ and the flows achieve a steady state by $t = 40$ days, although the zonally invariant flows arrive at a steady state more quickly.

Equations (23) and (24) are solved using a split Lagrangian / spectral numerical method and all individual time integrations are performed using a fourth order Runge-Kutta method (RK4). An initial Lagrangian set of points is advected in the meridional overturning circu-

lation, $(\overline{v}, \overline{w})$ for a time Δt; the first equation in (24) is solved with Π_X and $\overline{S_u}$ set to zero. Then the zonal velocity is interpolated onto the original, regularly spaced grid and its meridional average is taken; the MATLAB routine TriScatteredInterp is used for interpolation. The zonal/vertical Fourier transform of $\langle \overline{u} \rangle$, $\langle \tilde{\overline{u}} \rangle$ and the Fourier transform of the pressure, $\tilde{\Pi}$, are advanced through a time step Δt by solving the first, fourth and fifth equations in (24) with the meridional advection terms set to zero; this is the wave step. The two operations are performed again in reverse order and the result is averaged; this constitutes one step forward in time. Because of the nature of the operator splitting, the commuting and averaging, one can show that this routine is second order in time. All computations (except the zonally invariant examples) are run with 32x32x16 grid points with a time step of 1/24; $\Delta X = 1250\,\text{km}$, $\Delta y = 187.5\,\text{km}$, $\Delta z = 1\,\text{km}$, $\Delta t = 1\,\text{hour}$.

a. Zonally invariant heating

In each of these examples, one of the three meridional heating profiles shown in figure 2 is turned on at time $t = 0$ and the zonal velocity is allowed to run until a steady state is apparent; the steady state is attained after 20 days. For the simulations, we have used a heating rate with maximum of 1 in non-dimensional units, corresponding to a maximum heating rate of 33 Kelvin/day and vertical velocity of 5 cm/s.

The amplitudes of the resulting zonal winds are plotted in figures 3 (a), (b) and (c) and correspond well to the zonally averaged jets in the tropics (Peixoto and Oort 1992). Furthermore, the wind profile is qualitatively consistent with the zonal winds in the tropics with subtropical westerlies and tropical easterlies. The winds above the equator are weak in

all of the examples, corresponding to easterlies of less than 5 m/s. There are weak westerlies above the off-equatorial heating maximum in the example corresponding to Boreal winter heating, figure 3 (c). It could be argued that the symmetric heating/asymmetric cooling example (figure 3 b) is better at capturing the qualitative features of the Boreal winter zonal winds than is the off-equatorial heating example in figure 3 (c). This is consistent with the notion that the subtropical terminus of the Hadley cell is determined by baroclinic instability.

b. Zonally localized heating

An effective way to generate a gravity wave response is to completely zonally localize the heating. We again consider equinox heating (top frame of figure 2), but with a zonally localized spatial profile $S \propto e^{-\frac{X^2}{2a^2}}$ with $a = 2^{-\frac{1}{2}}$. Recall that X is measured in units of 5000 km, so the zonal extent of the heating, a, corresponds to ± 3500 km from the center of the heating. We choose a maximum amplitude of 2 for this example, corresponding to 66 Kelvin/day or 10 cm/s at the location of the maximum heating. Results (not shown) for the same zonal heating profile, but with solstice heating are qualitatively the same as those of equinox heating with the exception of the meridional location of the jets; essentially these are the differences between figures **??** and 3.

For the equinox heating example, the zonal velocity is plotted in figure 4 at the top, middle and bottom of the troposphere after 40 days; it has approximately reached a steady state by this time. It is clear that the variation in zonal winds are confined near the heating region, however away from the heating, the zonal winds are non-zero because of the passing of the gravity wave.

To see this more clearly, figure 5 shows the zonal-time plot of the meridional mean zonal wind evaluated at the top of the troposphere. A wave is seen to emanate from the origin in both directions, returning to the origin after 8 days (which is consistent with the dry gravity wave speed of 50 m/s). After sloshing through the atmosphere several more times, the upper troposphere is almost finished evolving at 40 days. It is clear that the mean winds in the upper troposphere are about 10 m/s outside the forcing region, and slightly lower inside the forcing region.

The meridional mean of the zonal velocity is plotted after 2, 8 and 40 days in figure 6. After 2 days, the gravity bore which is generated, travels away from the convective region carrying mean easterlies in the lower troposphere and mean westerlies in the upper troposphere. Since the flow is vertical/zonal incompressible, the bore carries a front of downward (secondary) flow in the middle troposphere to the east of the convection and a front of upward flow to the west of the convection. In its horizontal (x,z) profile, the bore looks like a clockwise rotating roll, with westerlies at the top of the troposphere and easterlies at the bottom, whose zonal extent increases until it intersects with itself at the antipode of convection.

As is shown in the discussion section (see figure 12) the wave also carries a temperature perturbation which is positive to the east of the convection and negative to the west; this temperature asymmetry is explained in the discussion section below. The temperature perturbation is shown in figure 7 at times 1, 4 and 40 days. After the flow equilibrates, the temperature perturbation remains since it is in hydrostatic equilibrium with the pressure which is needed to balance the advection and drag terms in the zonal momentum equation.

That convection is "gregarious" has been noted by authors since Mapes (1993) (Houze

1997). It is understood that gravity waves propagating away from a convective region carry temperature and divergence signals which tend to excite convection in the immediate environment. Models by Stechmann and Majda (2009) have shown that vertical shear can influence the location of the subsequent convective elements relative to the original ones. This example of M-ITCZ suggests another mechanism at work; the establishment of meridional mean upper tropospheric westerlies excites a gravity bore whose temperature and vertical velocity perturbations are favorable to exciting convection to the west of the original convection while suppressing it to the east. Since this is an aspect of the planetary scale equations we conclude that there is the possibility of coupling convection at very large *westward* zonal displacements in the tropics.

After 8 days (figure 6) the wave has returned to the convective source, and the zonal velocity contours have begun to flatten out. At 40 days, the flow is essentially in its steady state. The contours outside of the heating region are flat, corresponding to no variation in the vertical shear. The contours within the heating region all move upward in concert with one another, also corresponding to no variation in vertical shear. At a given height, the meridional mean zonal wind is weaker inside the heating region than it is outside this region.

c. Zonally localized, lower tropospheric heating

In the lower troposphere heating example we use a maximum heating strength and meridional profile equal to that of the middle troposphere example in order to make a direct comparison. The equilibrium zonal winds are shown in figures 8 (compare with figure 4). It is clear that the upper tropospheric winds are much weaker in this example whereas the lower

tropospheric winds are much stronger, reaching amplitudes of 20 m/s. This is also evident in figure 9 where the maximum mean winds of 10 m/s are achieved at the height of 10 km.

Figure 10 shows the longitude-time plot of the meridional mean winds at the top of the troposphere and there is a marked difference between it and figure 5. Comparing the structure of the contours between 5 and 16 days a second, slower wave traveling at 25 m/s is evident in this figure. In figure 5, the eastward and westward wave collide at $X = 0$ at 8 days. In this lower tropospheric heating example, there is a wave collision at 8 days, but it is broad in time, extending beyond 15 days. One notes the spreading of the contours from 5 days at the antipode of convection until 16 days; such spreading was not evident in figure 5. This slower wave is the signature of the stronger second baroclinic zonal velocity mode which is generated by the imposed second baroclinic heating in this congestus example. The non-monotonicity of the zonal velocity as a function of height in figure 9 is also a result of the second baroclinic heating. The second baroclinic mode is very clearly evident in the temperature profile in figure 11 where there is a cold (warm) perturbation in the upper troposphere above the warm (cold) perturbation in the lower troposphere. Most importantly for the purposes of convective coupling, the temperature perturbation in this example is double that of the mid-tropospheric heating example, 10 K in this case. Furthermore, the temperature maximum is located at heights of 3 km, compared to 4 km in the mid-troposphere heating example. Note that congestus heating carries low level easterlies with cooler temperature in the lower troposphere to the west of the convection just as in the example from figure 5. Such strong, lower troposphere temperature perturbations would have a significant effect on convectively coupled waves.

4. Discussion

a. The gravity wave explained as a forced linear wave

We can see the effect of the gravity wave if we consider a first baroclinic model

$$\begin{aligned} \langle \overline{u} \rangle &= \tilde{u}\cos(z), \qquad W = -\tilde{u}_X \sin(z), \\ \Theta &= \tilde{\Theta}\sin(z), \qquad \Pi = -\tilde{\Theta}\cos(z) \end{aligned} \tag{26}$$

where we have used the hydrostatic and incompressibility constraints in equations (24) to write the pressure and vertical velocity in terms of the temperature and zonal velocity. Outside of the convective region $\bar{v} = \bar{w} = 0$, so the gravity wave equations become

$$\begin{aligned} \tilde{u}_t - \tilde{\Theta}_X &= 0 \\ \tilde{\Theta}_t - \tilde{u}_X &= 0 \end{aligned} \tag{27}$$

which are simply the wave equation written as a system of first order equations. To solve these equations, initial data must be prescribed; initial zonal velocity, $\tilde{u}_0(X)$, and temperature, $\tilde{\Theta}_0(X)$, however, for the problem we are considering, the initial data is all zero.

Imagine a region of convection at $X = 0$ in the limit that its zonal extent becomes thin while its amplitude becomes large, so that the integrated heating remains constant (a Dirac delta function). We can think of $X = 0$ as an internal boundary where convective heating drives a meridional circulation which, in turn, drives a Coriolis acceleration, $\langle y\bar{v} \rangle$. Note that $\langle y\bar{v} \rangle < 0$ for a meridional flow that converges at the equator - which the Hadley cell does at the bottom of the troposphere. Therefore, the convection indirectly acts as source of zonal

momentum driving lower troposphere easterlies and upper troposphere westerlies at $X = 0$. Let us choose a simple zonal velocity profile at $X = 0$ to illustrate

$$\tilde{u}(0,t) = \begin{cases} -\tanh\left(\frac{t}{\tau}\right), & t \geq 0 \\ 0, & t < 0. \end{cases} \tag{28}$$

The solution of the wave equation for the zonal velocity, for all time, is

$$u(X,t) = -\tanh\left(\frac{t-|X|}{\tau}\right)\cos(z), \quad t \geq |X| \tag{29}$$

and is zero for $t \leq |X|$; this describes an expanding front. Using the zonal/vertical incompressibility constraint, the vertical velocity is

$$W(X,t) = -\frac{1}{\tau}\sigma(X)\,\mathrm{sech}^2\left(\frac{t-|X|}{\tau}\right)\sin(z), \quad t \geq |X|, \tag{30}$$

it is zero for $t \leq |X|$; $\sigma(X)$ is the sign of X. Therefore there is a downward pulse propagating to the east of the convection and an upward pulse to the west. The temperature is attained by integrating the first equation in (27)

$$\Theta(X,t) = \sigma(X)\tanh\left(\frac{t-|X|}{\tau}\right)\sin(z), \quad t \geq |X| \tag{31}$$

and is zero for $t \leq |X|$. Therefore there is a positive temperature front to the east of the convection and a negative temperature front to the west of the convection. In this simple setting, there is a temperature discontinuity at $X = 0$, but in the examples, this is smoothed

out by the zonal extent of the convective region near the origin.

A schematic illustration of the wave is shown in figure 12. The gravity bore sends lower tropospheric easterlies and upper tropospheric westerlies both east and west of the convection. By the incompressibility constraint in the zonal/vertical plane, on the front that propagates eastward, the upper tropospheric westerly zonal wind must be connected to the lower tropospheric easterly wind by a downward velocity perturbation. Conversely, on the front that propagates westward, incompressibility implies that the lower tropospheric easterlies must be connected to the upper tropospheric westerlies by an upward velocity perturbation. This whole feature looks like a long thin roll in the (X, z)-plane (see figure 12). As is shown in equation (31), the eastward front carries positive temperature anomalies (since the background potential temperature is higher in the upper troposphere) and the westward front carries negative temperature anomalies (since the background potential temperature is lower in the lower troposphere). Therefore the western front of the wave carries conditions favorable to exciting more convection, while the eastern front carries conditions which tend to suppress convection.

We have not discussed the effect of momentum forcing, $\overline{S}_u$ on the gravity wave, but this simplification of the wave process sheds some light on what the effect of momentum forcing would be. If we consider zonally localized momentum forcing in the limit of a small region, but with finite integral, then it can be thought of much like zonally localized convection - it spins up zonal velocity in this region. Momentum forcing comes in one of two general forms, upscale fluxes or downscale dissipation from the Reynold's stress terms, $F^u = -\left(\overline{v'\,u'}\right)_y - \left(\overline{w'\,u'}\right)_z$ in equation (3). First we discuss the possible effect of these eddy momentum flux divergences in general. For simplicity consider the equations in (4) for the

555 mesoscale fluctuations, (u', v') without source terms so that $w' = 0$. These equations allow
556 arbitrary vertical structure with β-plane Rossby wave dispersion and can be expected to
557 generate active meridional and vertical variation at large scales through momentum fluxes
558 in the meridional direction, $\overline{(v'u')}_y$.

559 Next we briefly discuss the effect of these eddy fluxes on the meridional mean zonal
560 velocity. On taking the meridional mean of the Reynold's stress, and using the no meridional
561 flux boundary condition we see that the only remaining forcing term is the mesoscale vertical
562 transport of zonal momentum, $\langle F^u \rangle = -\left\langle \overline{w'\,u'} \right\rangle_z$. This term is a crucial ingredient in the
563 IPESD multiscale models of the Madden-Julian oscillation (Biello and Majda 2005, 2006).
564 It was noted there that if convection has a westward tilt with height, then the flux $\langle F^u \rangle$
565 drives westerlies in the lower troposphere and easterlies in the upper troposphere. In the
566 context of the M-ITCZ theory, such an upward/westward tilt would drive easterlies at the
567 top of the troposphere and westerlies at the bottom, which is exactly the opposite effect of
568 the Coriolis acceleration due to heating, $\langle y\bar{v} \rangle$. Therefore, in this example, a gravity bore
569 would propagate away from the forcing region and tend to excite convection to the *east*
570 of the forcing and suppress convection to the west. Though it is pure speculation at this
571 point, this fact may have importance for the eastward propagation of the MJO, or simply
572 for convectively coupled Kelvin waves.

573 *b. Comparison of the M-ITCZ and Matsuno-Gill prescribed heating models*

574 It is interesting to compare and contrast the M-ITCZ models in (1), (3) and summarized
575 in (24) with the traditional Matsuno-Gill models with prescribed heating. A systematic

multi-scale derivation of the regime of validity of the Matsuno-Gill model has been given by Biello and Majda (2005, 2006, 2010). Let x, y, t be measured in units of the equatorial synoptic scale, $L_E \approx 1500\,\mathrm{km}$ and let S_{MG} denote the heat source for the Matsuno-Gill model while S_θ from equation (1) denotes the non-dimensional heat source in the M-ITCZ model. For S_{MG} Biello and Majda (2005, 2006, 2010) show that

$$S_{MG}(x, y, z, t) \sim 10\ \mathrm{K/day} \tag{32}$$

in order for the Matsuno-Gill model to be valid. This means that the Matsuno-Gill model is able to describe synoptic scale dynamics with diabatic heat sources having strengths of $10\,\mathrm{K/day}$ when resolved on the synoptic scales. MK and Biello and Majda (2010) show that linear Matsuno theory does not apply on zonal planetary scales for dynamics on longer timescales than the equatorial time of 8 hours. For such large scale/longer time phenomena (such as the MJO), the dynamics are forced by upscale fluxes of momentum *and* advection by the Hadley circulation and the trade winds.

In contrast, the M-ITCZ heating model in equation (1) allows a mesoscale heating

$$S_\theta(\epsilon^{-\frac{1}{2}}x, \epsilon^{-\frac{1}{2}}y, z, \epsilon^{\frac{1}{2}}t). \sim 33\,\mathrm{K/day} \tag{33}$$

We have shown that, if the mesoscale means, $\bar{S}_\theta$ are of the same strength as the fluctuations (or if there are mesoscale means of the Reynolds stresses) a large scale gravity bore is generated in M-ITCZ. Thus the allowed heating in the M-ITCZ model is much stronger, yet more meridionally confined than the weaker and larger scale heating in the Matsuno-

Gill model. The M-ITCZ also induces a stronger vertical circulation of 5 cm/s compared with allowed Matsuno-Gill vertical velocities of 1.7 cm/s (Biello and Majda 2005). This has profound impact for the dynamics of the ITCZ model: first the β-plane effect of rotation is present, but much weaker in the M-ITCZ theory since in (24) the meridional velocity is determined by the heating and provides only a source term through the β-effect for the dynamically evolving zonal momentum. Since the effect of rotation is indirect and passive, a zonal pressure gradient drives meridionally averaged large scale zonal gravity waves which can propagate both east and west. In the same manner as the large scale linear Matsuno waves are advected by the mean circulation (Biello and Majda 2010), so too will the manifestation of this gravity wave outside of the tropics be affected by the large scale circulation there. In particular, we expect that the mean zonal winds, which are larger than 5 m/s away from the ITCZ will have an important effect on the structure and excitation of the ITCZ gravity waves.

In contrast, the weaker large scale heating in the Matsuno-Gill model, varying meridionally on the equatorial synoptic scale, creates dynamics where the equatorial β-effect is inherently coupled; the result is non-dispersive equatorial Kelvin waves which can only propagate eastward having a very specific meridional structure (Matsuno 1966; Majda 2003). Superficially, both the M-ITCZ model and the Matsuno-Gill model have eastward propagating gravity waves with a similar allowed zonal structure, however the amplitude, meridional scale and meridional structure are completely different; for these same reasons, M-ITCZ has westward propagating gravity waves which are non-dispersive with a structure which is completely different than the dispersive westward interio-gravity waves of the Matsuno-Gill theory (Majda 2003).

c. Summary and future work

We have described the mesoscale equatorial weak temperature gradient theory with the addition of a zonally propagating gravity wave. Although MEWTG is a multiscale theory, there is no separation of scales between the planetary and mesoscales. However, some simplification can be attained by splitting the flows into mesoscale means and fluctuations and considering the fluctuations as prescribed or parametrized.

On neglecting all upscale fluxes, we studied the effect of tropical diabatic heating (due to convection) on the zonal winds and the gravity wave that is generated. The most important effect of the gravity wave is to equalize the meridional mean of the vertical shear of zonal wind at all longitudes in the deep tropics. The carrier of this information is the gravity wave, which propagates cold temperature and upward velocity perturbations west of the convective signal, and the opposite to the east. In a model coupled to an active diabatic heat source, such a wave would tend to favor convection to the west of the original source. The height of convection would modify the structure of the gravity wave, changing the height of the maximum temperature perturbation and the speed with which it travels. For example, the stratiform signal of convection (2nd baroclinic mode) propagates more slowly than the deep signal (1st baroclinic mode) which can have important consequences for the direction and phasing of subsequent convective activity (Mapes 1993; Houze 1997; Stechmann and Majda 2009).

The M-ITCZ equations couple mesoscale, convectively generated Rossby waves with planetary scale gravity waves in the ITCZ. The existence of this westward propagating, non-dispersive gravity wave is generally precluded by linear equatorial wave theory. However,

as we show in the derivation of M-ITCZ, meridional geostrophic balance is neither valid at very low latitudes nor if the strength of the temperature perturbation is large enough. Interestingly, such a coupled westward propagating wave was seen in the observational analysis of Yang et al. (2003). A model which prescribes some moist dynamics (a closure for S_θ) would yield a mesoscale forced Rossby wave strongly tied to the slowed (through moisture coupling), westward propagating gravity wave.

In a future paper we will describe exactly such a coupling of the wave to an active diabatic heat source in order to generate the convectively coupled gravity and Rossby wave. It is also important to have a dynamic cooling offset the heating in $\overline{S}_\theta$, this would allow the poleward extent of the overturning circulation to modulate with latitude. Comparisons can be made between a closure which emphasizes dry baroclinic instability (Korty and Schneider 2008), versus ones which emphasize radiative cooling (Held and Hou 1980) or moisture transports (Pauluis et al. 2008).

A numerical routine to integrate the mesoscale dynamics has been developed by B. Khouider (U. Victoria). This will provide a direct numerical simulation to understand the effects of the large scale flows, $\overline{u}, \overline{v}, \overline{w}, \Theta$ on the upscale fluxes. In particular, the modulation of the zonal velocity and temperature perturbation can excite convective instability (through uplift and cooling) or suppress convection (through vertical wind shear).

A potential future application involves a convectively coupled version of the M-ITCZ theory, which would couple the westward traveling planetary scale gravity wave with embedded mesoscale barotropic Rossby waves. The resulting wave is a candidate for the easterly waves observed in the Eastern Pacific ITCZ (Yang et al. 2003; Serra et al. 2008). In fact, Yang et al. (2003) noted that the meridional structure (of velocity and geopotential height)

of the westward propagating waves over the Eastern pacific had a profile consistent with a nondispersive eastward propagating Kelvin wave; yet such waves are precluded by meridional geostrophic balance in the linear theory of equatorial waves (see, for example Biello and Majda (2006)). The derivation of the M-ITCZ theory explains that such a non-dispersive, westward propagating gravity wave arises because meridional geostrophic balance does not play a role on these scales.

Finally, in the derivation of the M-ITCZ theory, we found that it is valid up to distances $L_* \sim O(1)$ and we used $L_* = 6$ (which corresponds to 3000 km poleward) in our simulations. In the actual atmosphere the tropical dynamics must be coupled to midlatitudes and this poses a subtle issue, should L_* depend on X? What midlatitude scales are appropriate? Can the MEWTG gravity wave couple to midlatitude Rossby waves through their interaction in the subtropical jet? The resolution of these questions will also be discussed in a future paper.

5. Figures and tables

a. Figures

Acknowledgments.

J.A. Biello is supported by a National Science Foundation grant, DMS-1009959. A.J. Majda is partially supported by NSF grants DMS-0456713 and DMS-1025468 and by Office of Naval Research grants ONR DRI N0014-10-1-0554 and N0014-11-1-0306.

679

680 # REFERENCES

681 Biello, J. and A. Majda, 2004: Boundary layer dissipation and the nonlinear interaction of
682 equatorial baroclinic and barotropic Rossby waves. *GEOPHYSICAL AND ASTROPHYS-*
683 *ICAL FLUID DYNAMICS*, **98 (2)**, 85–127, doi:{10.1080/03091920410001686712}.

684 Biello, J. and A. Majda, 2005: A new multiscale model for the Madden-Julian oscillation.
685 *JOURNAL OF THE ATMOSPHERIC SCIENCES*, **62 (6)**, 1694–1721, doi:{10.1175/
686 JAS3455.1}.

687 Biello, J. A. and A. J. Majda, 2006: Modulating synoptic scale convective activity
688 and boundary layer dissipation in the IPESD models of the Madden-Julian oscilla-
689 tion. *DYNAMICS OF ATMOSPHERES AND OCEANS*, **42 (1-4, SI)**, 152–215, doi:
690 {10.1016/j.dynatmoce.2005.10.005}.

691 Biello, J. A. and A. J. Majda, 2010: INTRASEASONAL MULTI-SCALE MOIST DYNAM-
692 ICS OF THE TROPICAL ATMOSPHERE. *COMMUNICATIONS IN MATHEMATICAL*
693 *SCIENCES*, **8 (2)**, 519–540.

694 Bretherton, C. and A. Sobel, 2003: The Gill model and the weak temperature gradient
695 approximation. *JOURNAL OF THE ATMOSPHERIC SCIENCES*, **60 (2)**, 451–460, doi:
696 {10.1175/1520-0469(2003)060⟨0451:TGMATW⟩2.0.CO;2}.

697 Burns, S. P., A. H. Sobel, and L. M. Polvani, 2006: Asymptotic solutions of the ax-
698 isymmetric moist Hadley circulation in a model with two vertical modes. *THEORETI-*

699 *CAL AND COMPUTATIONAL FLUID DYNAMICS*, **20 (5-6)**, 443–467, doi:{10.1007/
700 s00162-006-0024-z}.

701 Chang, C.-P., 1970: Westward propagating cloud patterns in the tropical Pacific as seen
702 from time-composite satellite photographs. *J. Atmos. Sci*, **27**, 133–138.

703 Chang, C.-P., 1973: A dynamical model of the Intertropical Convergence Zone. *J. Atmos.*
704 *Sci*, **30**, 190–212.

705 Dolaptchiev, S., 2005: An asymptotic, nonlinear model for anisotropic, large-scale flows in
706 the tropics. *Postdam Institute for Climate Impact Research Report*, **101**.

707 Ferreira, R. N. and W. H. Schubert, 1997: Barotropic aspects of ITCZ breakdown. *J. Atmos.*
708 *Sci*, **54**, 261–285.

709 Gu, G. and C. Zhang, 2001: A spectrum analysis of synoptic-scale disturbances in the ITCZ.
710 *J. Climate*, **14**, 2725–2739.

711 Gu, G. and C. Zhang, 2002: Westward propagating synoptic scale disturbances and the
712 ITCZ. *J. Atmos. Sci*, **59**, 1062–1075.

713 Hack, J. J., , W. H. Schubert, D. E. Stevens, and K. Hung-Chi, 1989: Response of the
714 Hadley circulation to convective forcing in the ITCZ. *J. Atmos. Sci*, **46**, 2957–2973.

715 Held, I. and A. Hou, 1980: NON-LINEAR AXIALLY-SYMMETRIC CIRCULATIONS IN
716 A NEARLY INVISCID ATMOSPHERE. *JOURNAL OF THE ATMOSPHERIC SCI-*
717 *ENCES*, **37 (3)**, 515–533, doi:{10.1175/1520-0469(1980)037⟨0515:NASCIA⟩2.0.CO;2}.

718 Horinouchi, T., 2012: Moist Haldey Circulation: Possible role of wave-convection coupling
719 in aquaplanet experiments. *J. Atmos. Sci*, **69**, 891–907.

720 Houze, R., 1997: Stratiform precipitation in regions of convection: A meteorological para-
721 dox? *BULLETIN OF THE AMERICAN METEOROLOGICAL SOCIETY*, **78 (10)**,
722 2179–2196, doi:{10.1175/1520-0477(1997)078⟨2179:SPIROC⟩2.0.CO;2}.

723 Korty, R. L. and T. Schneider, 2008: Extent of Hadley circulations in dry atmospheres.
724 *GEOPHYSICAL RESEARCH LETTERS*, **35 (23)**, doi:{10.1029/2008GL035847}.

725 Lin, J., M. Zhang, and B. Mapes, 2005: Zonal momentum budget of the Madden-Julian
726 oscillation: The source and strength of equivalent linear damping. *JOURNAL OF THE*
727 *ATMOSPHERIC SCIENCES*, **62 (7, Part 1)**, 2172–2188, doi:{10.1175/JAS3471.1}.

728 Majda, A., 2003: *Introduction to PDEs and Waves for the Atmosphere and Ocean*. American
729 Mathematical Society.

730 Majda, A. and J. Biello, 2004: A multiscale model for tropical intraseasonal oscillations.
731 *PROCEEDINGS OF THE NATIONAL ACADEMY OF SCIENCES OF THE UNITED*
732 *STATES OF AMERICA*, **101 (14)**, 4736–4741, doi:{10.1073/pnas.0401034101}.

733 Majda, A. and R. Klein, 2003: Systematic multiscale models for the tropics. *JOURNAL*
734 *OF THE ATMOSPHERIC SCIENCES*, **60 (2)**, 393–408, doi:{10.1175/1520-0469(2003)
735 060⟨0393:SMMFTT⟩2.0.CO;2}.

736 Majda, A. J., 2007: New multiscale models and self-similarity in tropical convection. *JOUR-*
737 *NAL OF THE ATMOSPHERIC SCIENCES*, **64 (4)**, 1393–1404, doi:{10.1175/JAS3880.
738 1}.

739 Majda, A. J., M. Mohammadian, and Y. Xing, 2008: Vertically sheared horizontal flow with
740 mass sources: a canonical balanced model. *GEOPHYSICAL AND ASTROPHYSICAL*
741 *FLUID DYNAMICS*, **102 (6)**, 543–591, doi:{10.1080/03091920802044787}.

742 Mapes, B., 1993: GREGARIOUS TROPICAL CONVECTION. *JOURNAL OF THE AT-*
743 *MOSPHERIC SCIENCES*, **50 (13)**, 2026–2037, doi:{10.1175/1520-0469(1993)050⟨2026:
744 GTC⟩2.0.CO;2}.

745 Matsuno, T., 1966: Quasi-geostrophic motions in the equatorial area. *J. Meteorol. Soc. Jpn.*,
746 **44**, 25–43.

747 Pauluis, O., A. Czaja, and R. Korty, 2008: The global atmospheric circulation on moist
748 isentropes. *SCIENCE*, **321 (5892)**, 1075–1078, doi:{10.1126/science.1159649}.

749 Peixoto, J. and A. Oort, 1992: *Physics of Climate*. American Institute of Physics, New York.

750 Polvani, L. and A. Sobel, 2002: The Hadley circulation and the weak temperature gradient
751 approximation. *JOURNAL OF THE ATMOSPHERIC SCIENCES*, **59 (10)**, 1744–1752,
752 doi:{10.1175/1520-0469(2002)059⟨1744:THCATW⟩2.0.CO;2}.

753 Serra, Y. L., G. N. Kiladis, and M. F. Cronin, 2008: Horizontal and vertical structure of
754 easterly waves in the Pacific ITCZ. *J. Atmos Sci*, **65**, 1266–1284.

755 Sobel, A., J. Nilsson, and L. Polvani, 2001: The weak temperature gradient approximation
756 and balanced tropical moisture waves. *JOURNAL OF THE ATMOSPHERIC SCIENCES*,
757 **58 (23)**, 3650–3665, doi:{10.1175/1520-0469(2001)058⟨3650:TWTGAA⟩2.0.CO;2}.

758 Stechmann, S. N. and A. J. Majda, 2009: Gravity Waves in Shear and Implications for

759 Organized Convection. *JOURNAL OF THE ATMOSPHERIC SCIENCES*, **66 (9)**, 2579–
760 2599, doi:{10.1175/2009JAS2976.1}.

761 Wang, C.-C. and G. Magnusdottir, 2006: The ITCZ in the central and eastern Pacific on
762 synoptic time scales. *Mon. Weather Rev.*, **134**, 1405–1421.

763 Yang, G.-Y., B. Hoskins, and J. Slingo, 2003: Convectively coupled equatorial waves: a new
764 methodology for indentifying wave structures in observational data. *J. Atmos. Sci*, **60**,
765 1637–1654.

List of Figures

1 A schematic depiction of the multiscale domain. The variables (x, y) measure zonal and meridional displacements within a mesoscale box. The variable X measures the planetary scale over which the behavior of each of the individual mesoscale boxes can be modulated, $X = 1$ corresponds to 5000 km in the zonal direction. This modulation is caused by, both, the variation of the heating rate on the planetary scale, and the gravity wave generated by the onset of convection in one mesoscale box. 48

2 The bottom panel shows meridional structure of the heating, S_θ (the amplitude is arbitrary) for the cases of equinox heating with symmetic (solid curve with peak at $y = 0$) and antisymmetric (dashed curve with peak at $y = 0$) cooling and boreal winter heating (sol curve with peak at $y = -1000$ km). The top three panels contour the stream function versus height and meridional distance from the equator for the three cases, respectively. Note, in all three cases, the heating occupies a width of 1000 km about the equator. . . 49

781 3 Zonal winds as a function of longitude and height for (a) the zonally symmet-
782 ric, equinox heating example (b) the equinox heating, but asymmetric cooling
783 example and (c) the boreal winter example ; the meridional overturning circu-
784 lation corresponds to the first three frames in figure 2, respectively. In (a) are
785 seen the sharp meridional gradient of the westerly zonal jets in the subtropics
786 and the easterlies at the bottom of the troposphere. In (b) the zonal winds
787 are weaker in the southern hemisphere, where the cooling is weaker. In (c)
788 the easterlies become stronger at the ground near the equator and there is are
789 weak westerlies up to the upper troposphere above the heating maximum at
790 $y = -1000\,\mathrm{km}$. 50
791 4 Contours of zonal velocity at the top, middle and bottom of the troposphere;
792 note that shading scale is different in the three plots. Easterlies are evident
793 in the lower troposphere near the equator, as are westerlies further poleward.
794 There are strong easterlies at the top of the troposphere above the equator,
795 as well as westerly zonal jets at 2000 km north/south. 51
796 5 Zonal space versus time plot of the meridional mean zonal wind for the
797 equinox, zonally localized heating profile. The gravity wave creates upper
798 troposphere westerlies. 52
799 6 Meridional mean zonal velocity as a function of (x, z) at 2, 8 and 40 days
800 for the equinox, zonally localized heating profile. The vertical velocity, W, is
801 upward on the western front and downward on the eastern front of the wave. 53

7 Temperature perturbation as a function of (x, z) at 1,4 and 40 days for the equinox, zonally localized heating profile. The vertical velocity, W, is upward on the western front and downward on the eastern front of the wave. 54

8 Contours of zonal velocity at the top, middle and bottom of the troposphere for the example of lower troposphere, equatorially symmetric but zonally localized heating; note that shading scale is different in the three plots. Easterlies are evident in the lower troposphere near the equator, as are westerlies further poleward. Now the strongest westerlies lie in the mid troposphere. 55

9 Meridional mean zonal velocity as a function of (x, z) at 2, 8 and 40 days for the lower troposphere heating profile. Maximum westerlies are located at 10 km and, after 40 days, the flow has yet to achieve a steady state. 56

10 Zonal space versus time plot of the meridional mean zonal wind for the lower troposphere, zonally localized heating profile. The lower tropospheric heating drives mean easterlies in the upper troposphere. Also evident is the signature of the second baroclinic wave, which circumnavigates the globe in 16 days. Compare the structure of this wave to that in figure 5; a clear second baroclinic signature is evident from days 5-16. 57

11 Temperature perturbation as a function of (x, z) at 1,4 and 40 days for the equinox, zonally localized heating profile. The maximum amplitude of the temperature perturbation is about 10 Kelvin, achieved at heights of 3 km. Compare with figure 7 where the maximum ampltiude is 5 Kelvin, achieved at heights of 4 km. 58

12 A schematic depiction of the wave of the M-ITCZ theory. Convection excites upper tropospheric mean westerlies and lower tropospheric mean easterlies. This drives a gravity bore eastward and westward. The wave to the east carries downward velocity and warm temperature perturbations. The wave to the west carries upward velocity and cold temperature perturbations, making it favorable to excite convection. 59

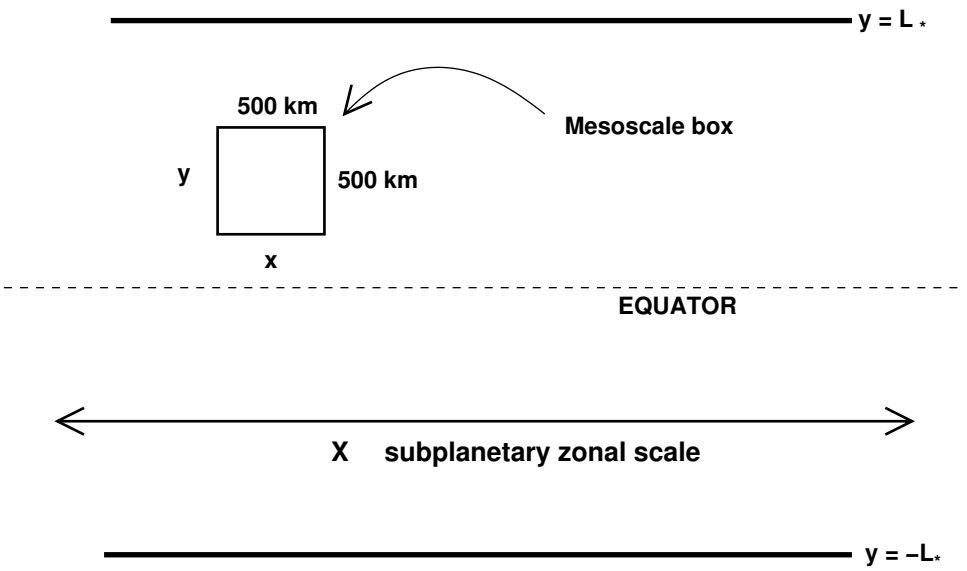

FIG. 1. A schematic depiction of the multiscale domain. The variables (x, y) measure zonal and meridional displacements within a mesoscale box. The variable X measures the planetary scale over which the behavior of each of the individual mesoscale boxes can be modulated, $X = 1$ corresponds to 5000 km in the zonal direction. This modulation is caused by, both, the variation of the heating rate on the planetary scale, and the gravity wave generated by the onset of convection in one mesoscale box.

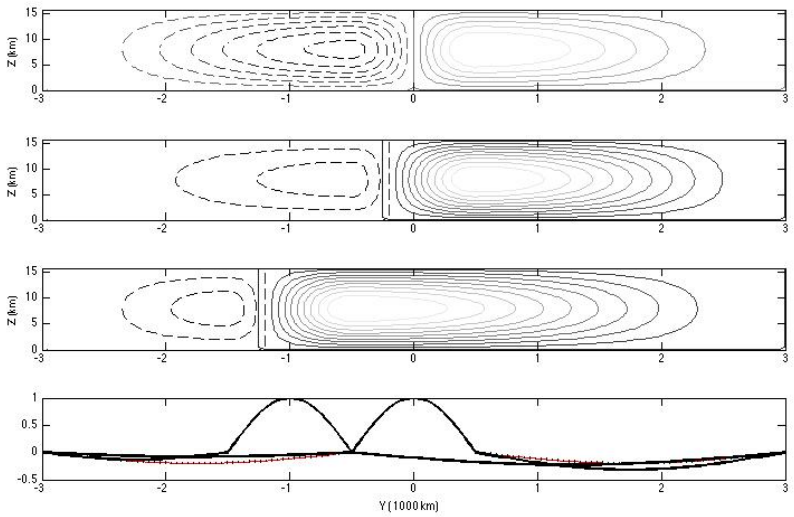

FIG. 2. The bottom panel shows meridional structure of the heating, S_θ (the amplitude is arbitrary) for the cases of equinox heating with symmetic (solid curve with peak at $y = 0$) and antisymmetric (dashed curve with peak at $y = 0$) cooling and boreal winter heating (sol curve with peak at $y = -1000$ km). The top three panels contour the stream function versus height and meridional distance from the equator for the three cases, respectively. Note, in all three cases, the heating occupies a width of 1000 km about the equator.

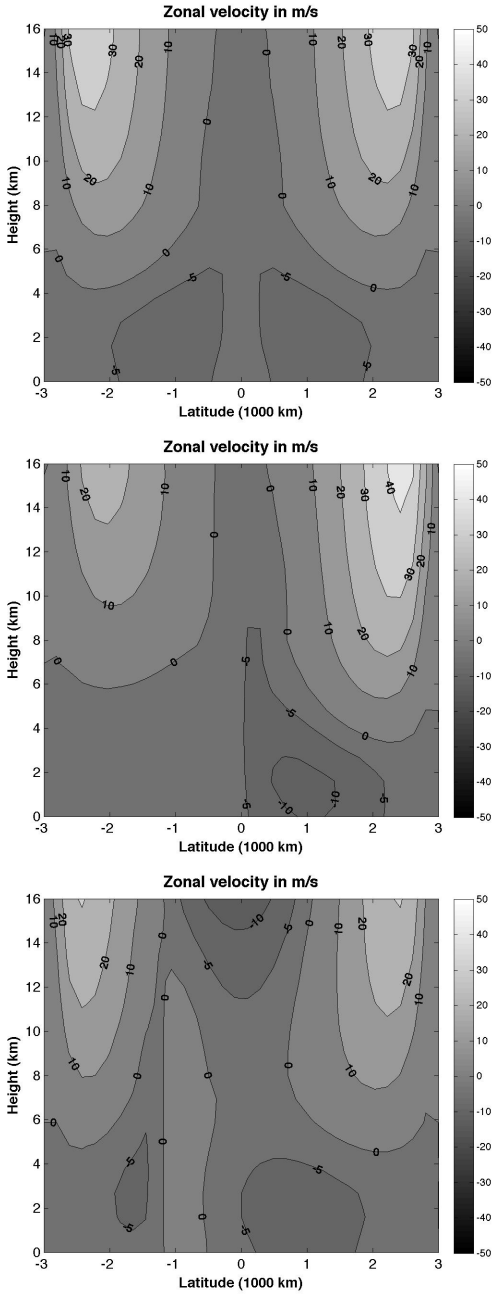

FIG. 3. Zonal winds as a function of longitude and height for (a) the zonally symmetric, equinox heating example (b) the equinox heating, but asymmetric cooling example and (c) the boreal winter example ; the meridional overturning circulation corresponds to the first three frames in figure 2, respectively. In (a) are seen the sharp meridional gradient of the westerly zonal jets in the subtropics and the easterlies at the bottom of the troposphere. In (b) the zonal winds are weaker in the southern hemisphere, where the cooling is weaker. In (c) the easterlies become stronger at the ground near the equator and there is are weak westerlies up to the upper troposphere above the heating maximum at $y = -1000\,\mathrm{km}$.

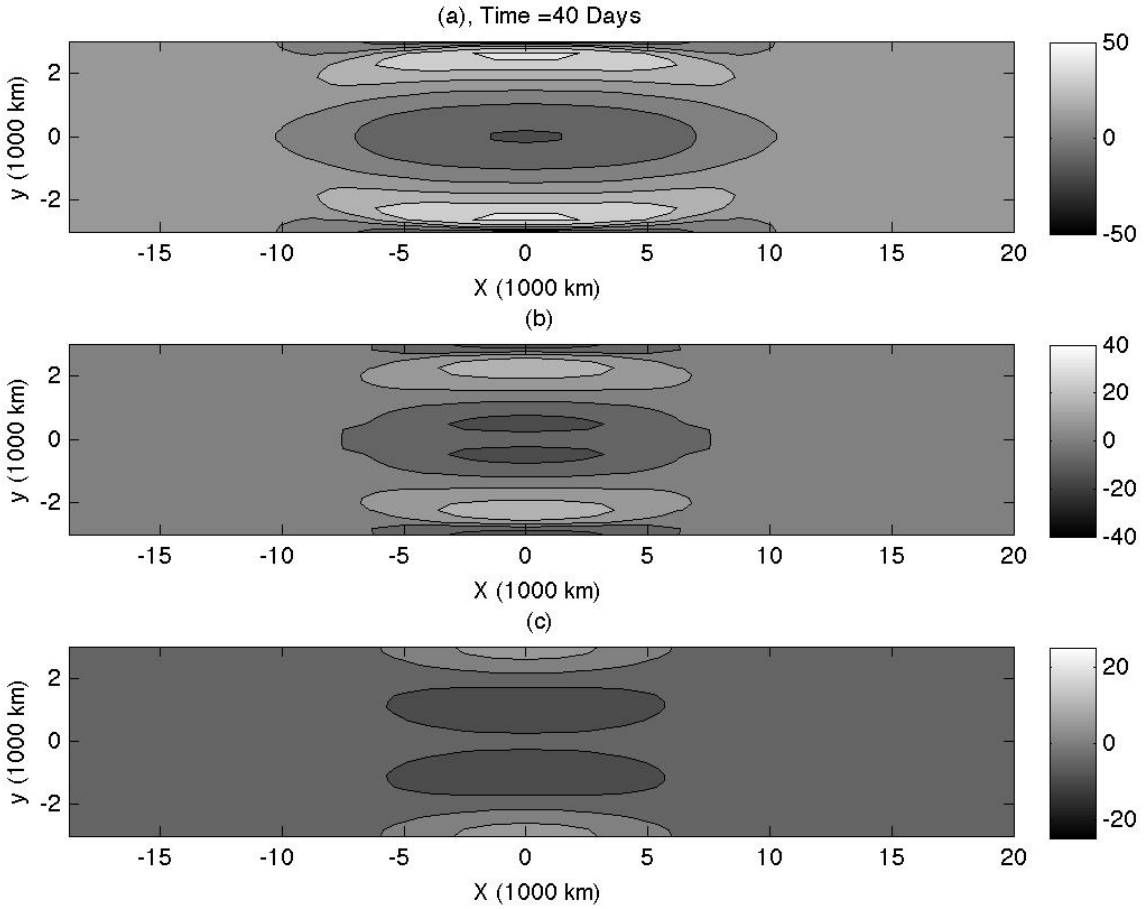

FIG. 4. Contours of zonal velocity at the top, middle and bottom of the troposphere; note that shading scale is different in the three plots. Easterlies are evident in the lower troposphere near the equator, as are westerlies further poleward. There are strong easterlies at the top of the troposphere above the equator, as well as westerly zonal jets at 2000 km north/south.

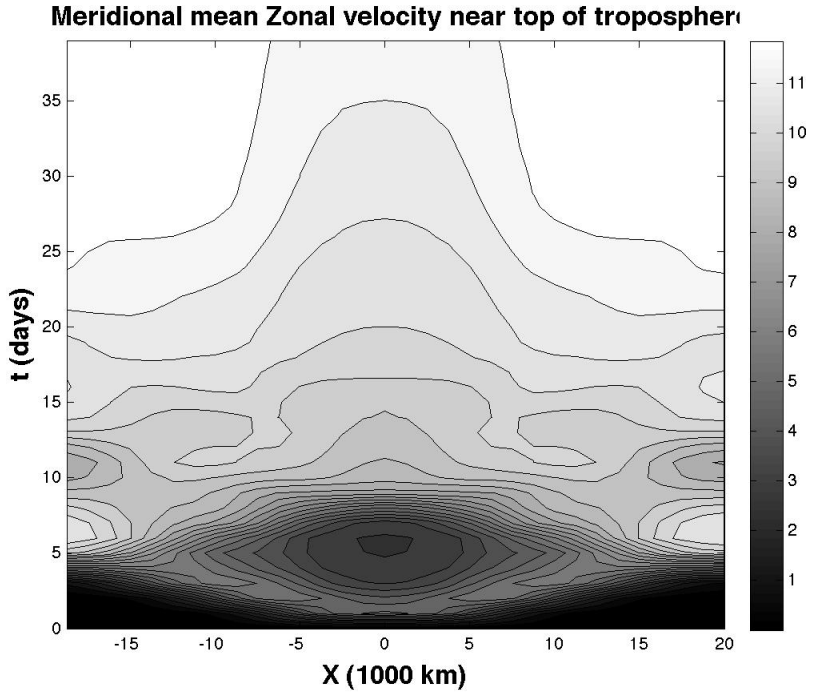

FIG. 5. Zonal space versus time plot of the meridional mean zonal wind for the equinox, zonally localized heating profile. The gravity wave creates upper troposphere westerlies.

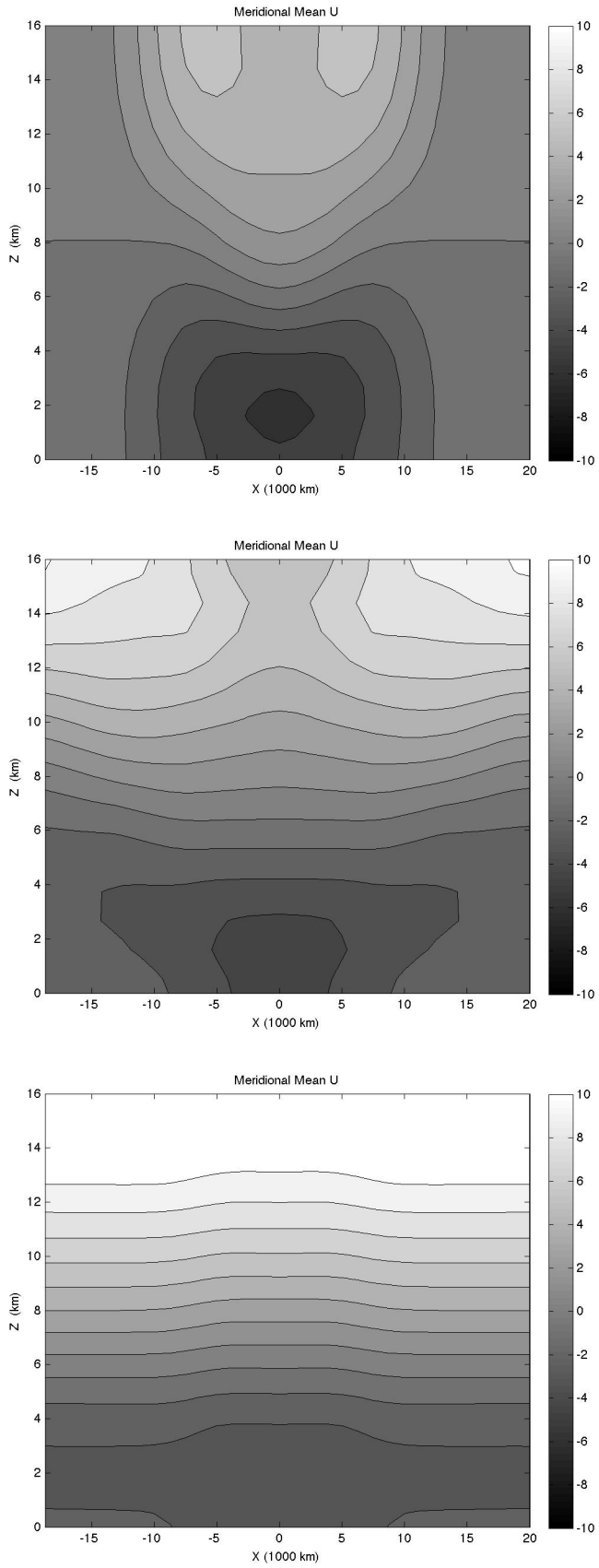

FIG. 6. Meridional mean zonal velocity as a function of (x, z) at 2, 8 and 40 days for the equinox, zonally localized heating profile. The vertical velocity, W, is upward on the western front and downward on the eastern front of the wave.

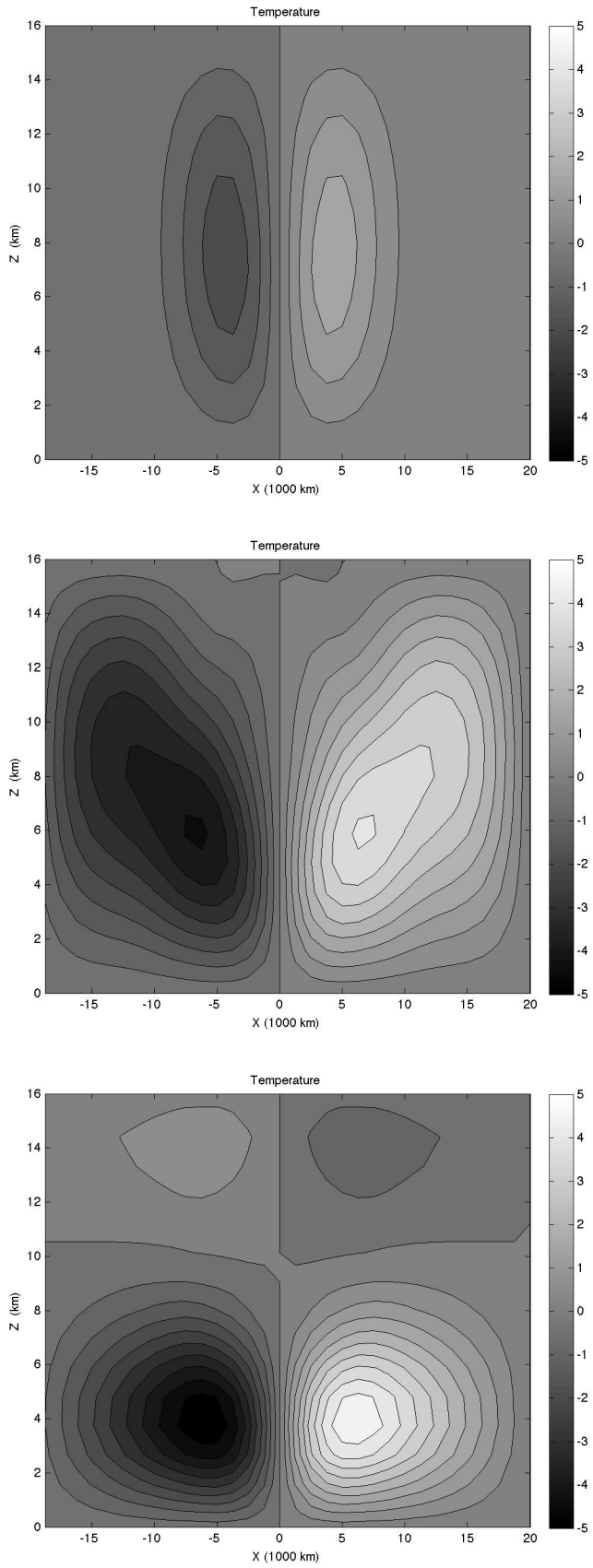

FIG. 7. Temperature perturbation as a function of (x, z) at 1,4 and 40 days for the equinox, zonally localized heating profile. The vertical velocity, W, is upward on the western front and downward on the eastern front of the wave.

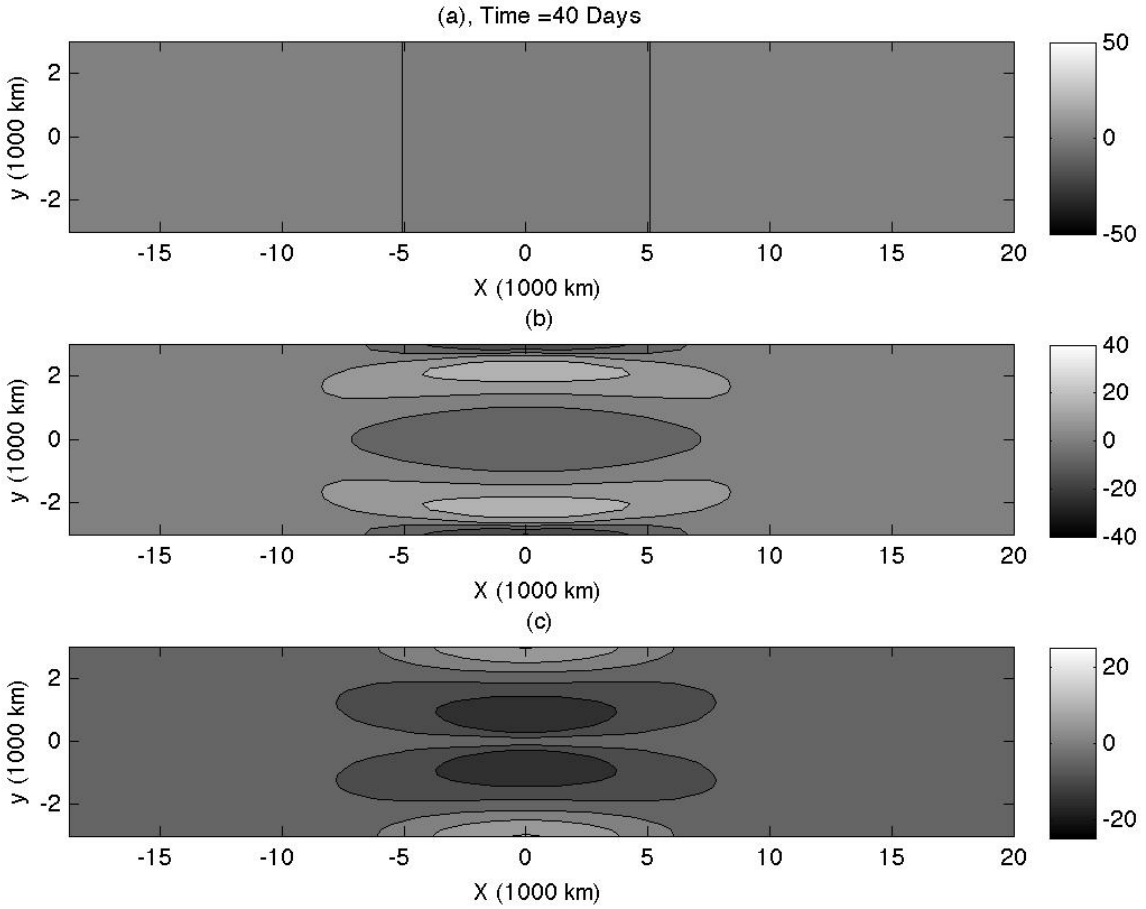

FIG. 8. Contours of zonal velocity at the top, middle and bottom of the troposphere for the example of lower troposphere, equatorially symmetric but zonally localized heating; note that shading scale is different in the three plots. Easterlies are evident in the lower troposphere near the equator, as are westerlies further poleward. Now the strongest westerlies lie in the mid troposphere.

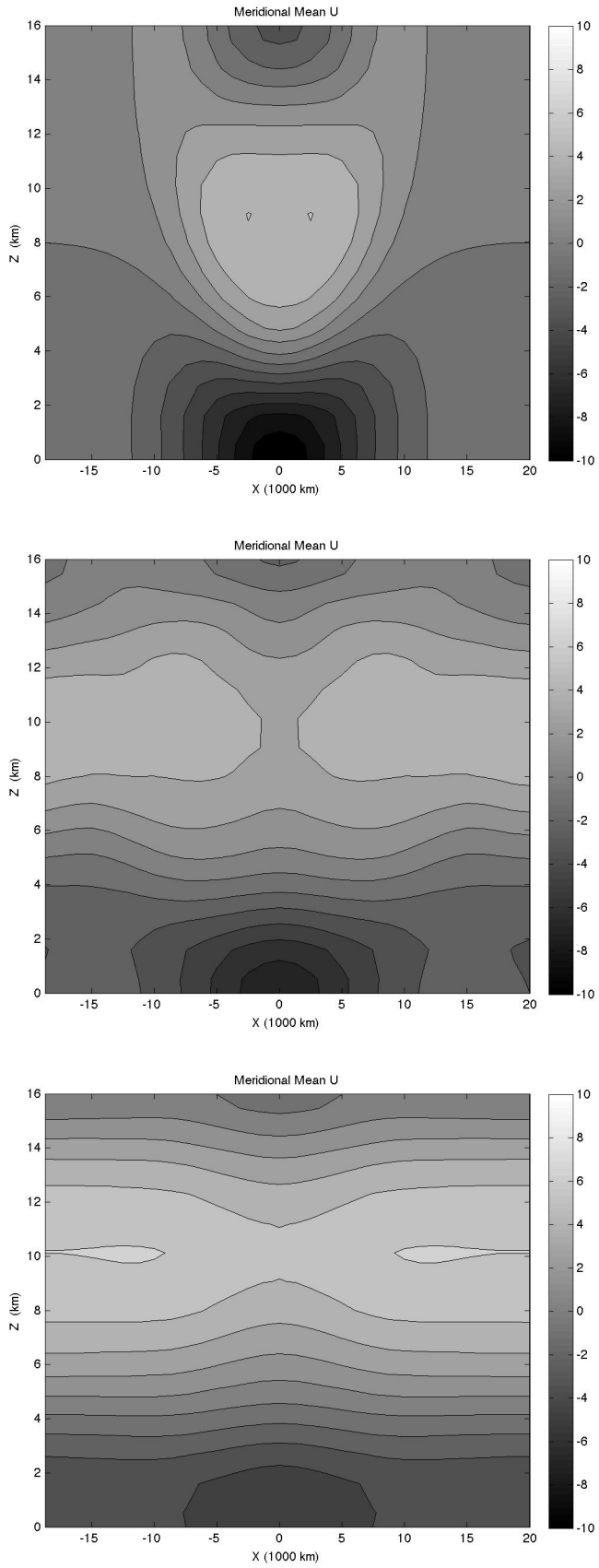

FIG. 9. Meridional mean zonal velocity as a function of (x, z) at 2, 8 and 40 days for the lower troposphere heating profile. Maximum westerlies are located at 10 km and, after 40 days, the flow has yet to achieve a steady state.

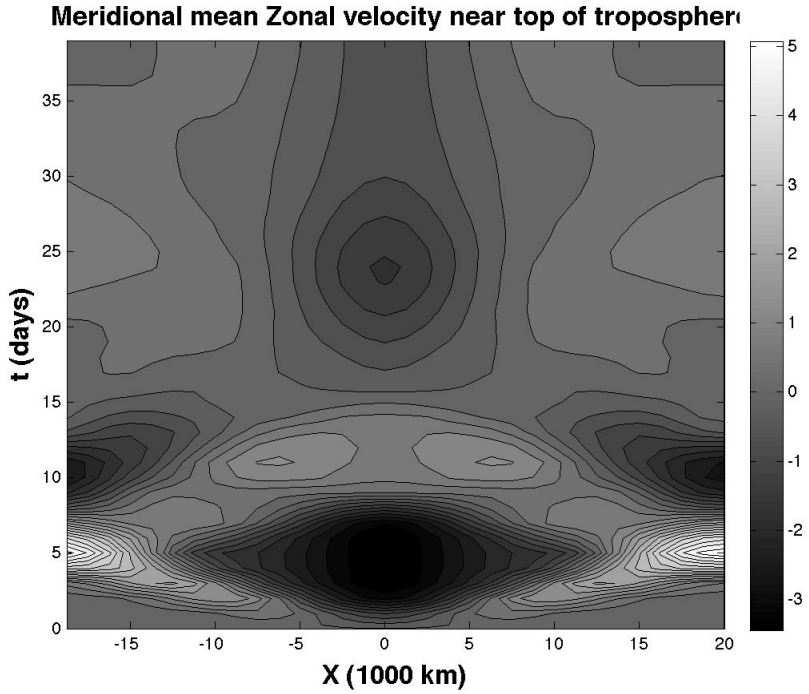

FIG. 10. Zonal space versus time plot of the meridional mean zonal wind for the lower troposphere, zonally localized heating profile. The lower tropospheric heating drives mean easterlies in the upper troposphere. Also evident is the signature of the second baroclinic wave, which circumnavigates the globe in 16 days. Compare the structure of this wave to that in figure 5; a clear second baroclinic signature is evident from days 5-16.

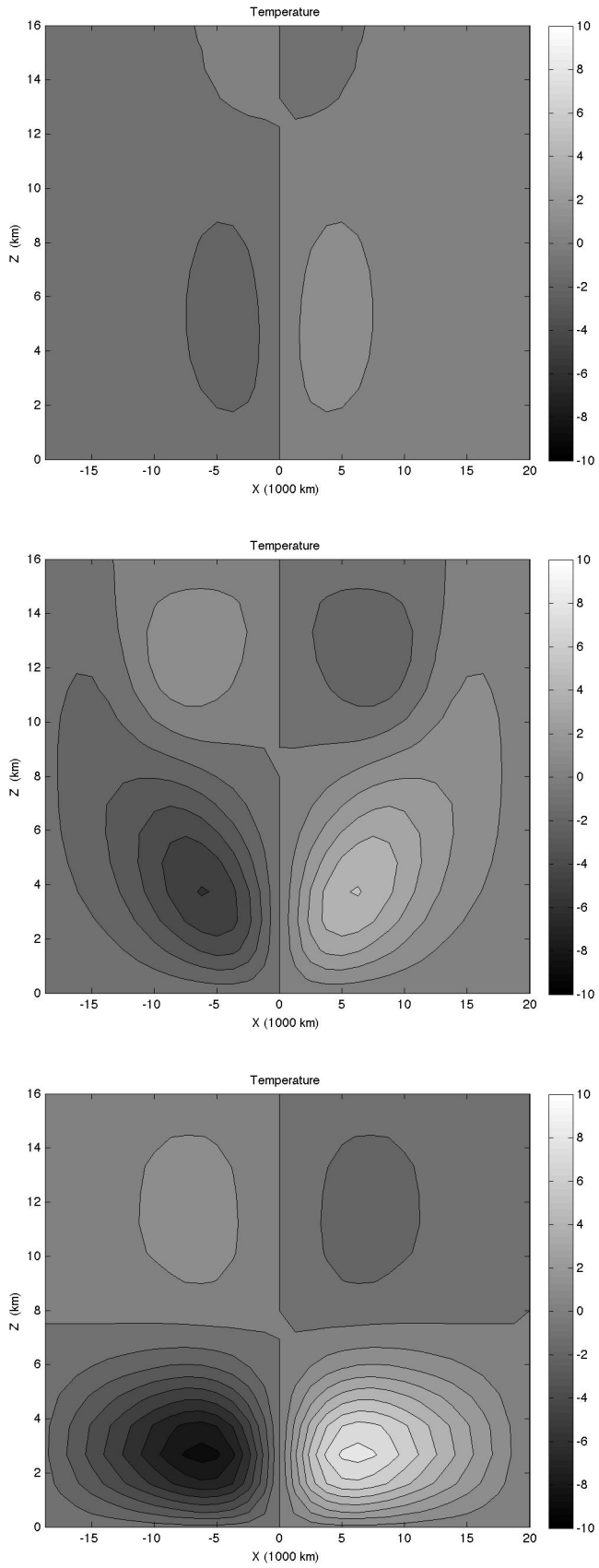

FIG. 11. Temperature perturbation as a function of (x, z) at 1,4 and 40 days for the equinox, zonally localized heating profile. The maximum amplitude of the temperature perturbation is about 10 Kelvin, achieved at heights of 3 km. Compare with figure 7 where the maximum ampltiude is 5 Kelvin, achieved at heights of 4 km.

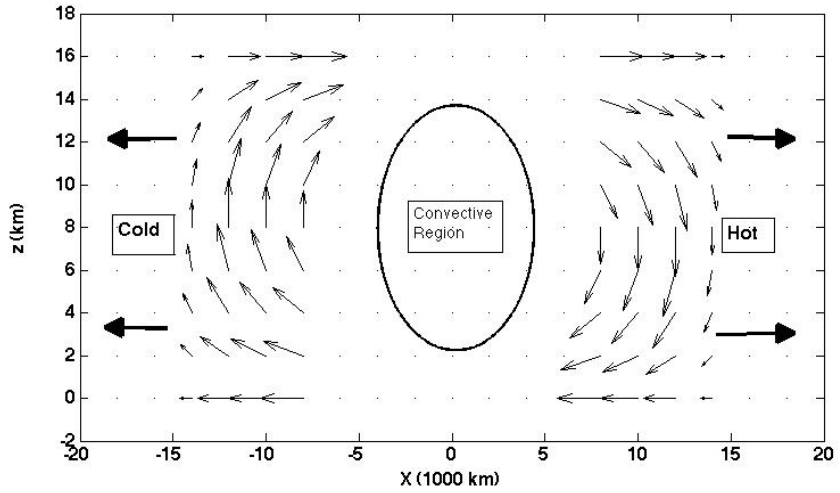

FIG. 12. A schematic depiction of the wave of the M-ITCZ theory. Convection excites upper tropospheric mean westerlies and lower tropospheric mean easterlies. This drives a gravity bore eastward and westward. The wave to the east carries downward velocity and warm temperature perturbations. The wave to the west carries upward velocity and cold temperature perturbations, making it favorable to excite convection.